



# Diphtheria transmission prediction by extended Kalman filter ☆,☆☆

Mohammad Ghani

*Data Science Technology, Faculty of Advanced Technology and Multidiscipline, Universitas Airlangga, Surabaya 60115, Indonesia*



## ARTICLE INFO

**Method name:**

Extended Kalman Filter

**Keywords:**

Diphtheria  
Transmission rate  
Isolation rate  
DPT  
Booster  
Extended Kalman filter

## ABSTRACT

Diphtheria transmission in West Java becomes our concern in this paper. The findings of this article are implementation of isolation and estimation technique of parameters using extended Kalman filter on the model of diphtheria transmission. From the eigenvalues of next generation matrix, the basic reproduction number is obtained. Then, the implementation of using extended Kalman filter provides the trend of the basic reproduction number of the diphtheria model with several cases: DPT only, Booster only, and a combination of DPT and booster. Based on the values of RMSE, NRMSE, and MAPE, the Extended Kalman Filter method provides significant results in estimating the basic reproduction number on actual data of diphtheria cases in West Java. We also studied the quarantined population in this article, because the rate of isolation has a significant impact on the profile of the susceptible, infected, quarantined, and recovered populations. Based on the results obtained, DPT only gives the smallest number when compared to Booster only and the combination of DPT and Booster. This is likely when DPT only is given, the body forms an immune system so giving Booster only does not provide significant results in reducing the level of effectiveness of diphtheria transmission (reducing the basic reproduction number).

- This paper purposes to get the prediction of diphtheria transmission by using Extended Kalman Filter.
- The basic reproduction number is also studied for the DPT only, booster only, and the combinations of DPT and booster.
- The Extended Kalman Filter shows the good performance based on the RMSE, NRMSE, and MAPE.

## Specifications table

Subject area:	Mathematics and Statistics
More specific subject area:	Data-Driven Dynamical Systems
Name of your method:	Extended Kalman Filter
Name and reference of original method:	None
Resource availability:	None

## Background

The spread of diphtheria in 2018 resulted in Extraordinary Events in 28 provinces and 142 districts/cities in Indonesia. Diphtheria is spread through the air and saliva by the bacteria *Corynebacterium diphtheriae*, causing respiratory tract infection. A sign of diphthe-

\* Related research article: None

\*\* For a published article: None

E-mail address: [mohammad.ghani@ftmm.unair.ac.id](mailto:mohammad.ghani@ftmm.unair.ac.id)

ria is that the pseudo membrane thickens, resulting in difficulty breathing [36]. The World Health Organization estimates that diphtheria can cause around 30 % of cases without proper vaccination and treatment. Diphtheria has a higher risk of death in children [32]. A majority of diphtheria cases in Nigeria occur in children between the ages of 2 and 14 [1]. As an Emerging disease, diphtheria was once under control but has reappeared with an increasing incidence rate. Based on the source <https://sehatnegeriku.kemkes.go.id/>, from 2019 to 2024 as many as 1.8 million Indonesian children did not receive routine immunization. As a result, Extraordinary Events in diphtheria occurred again in Indonesia. Indonesia's five largest islands with diphtheria cases are Java with 474 cases and 26 deaths, Sumatra with 114 cases and 5 deaths, Kalimantan with 13 cases and 1 death, Sulawesi with 11 cases, and Papua with one case [33]. Diphtheria was also reported in Bangladesh, Yemen, and Venezuela [7]. India suffered a 15 % death rate due to diphtheria outbreaks [21]. Among the most likely outcomes of 2022 is that toxigenic diphtheria will spread more rapidly [5]. North Queensland, Australia, also experienced an increase in toxigenic diphtheria cases [14]. Toxigenic diphtheria is caused by toxin-producing *Corynebacterium*, causing respiratory and skin problems [22]. Diphtheria cases are increasing/reemerging in Nigeria [27]. Diphtheria re-emerged in Pakistan after the Covid-19 pandemic, resulting in 124 deaths in all provinces [28].

The spread of a diphtheria outbreak can cause serious consequences if not treated quickly. For effective control strategies and outbreak prevention, it is crucial to understand how diphtheria spreads. Infectious diseases, including diphtheria, have been studied using mathematical models. Diphtheria spread model predictions can be used to identify vulnerable areas and implement appropriate preventive measures, including vaccine distribution, resource allocation, and health services. Mathematical modeling with diphtheria antibody decay and protection is predicted using long-term predictions [6]. According to a mathematical model of diphtheria outbreak in Thailand, vaccinations every 10 years will decrease the spread of the disease [31]. Using real-time modeling, we are able to determine the potential scale and scope of the epidemic, the resource requirements, and the transmission mechanisms of diphtheria [10]. The use of antibiotics can control diphtheria cases [16]. In Rohingya refugee camps in Bangladesh, diphtheria outbreaks have a basic reproduction ratio of 5.86, indicating a very high outbreak level [15]. The mathematical model of the spread of diphtheria with asymptomatic infection, logistic growth, and vaccination forms the  $S - V - E - A - I - R$  model [17]. The fractional model of diphtheria spread forms five compartments, namely  $S - E - I - Q - R$  [12]. The control strategy for predicting diphtheria cases using disinfection and booster vaccination can reduce the spread rate [20]. Vaccination, treatment, and interaction contact tracing demonstrate effective results in the diphtheria spread model [2]. The addition of booster vaccination of 75.15 % was able to control the spread of diphtheria [9]. Mathematical model for diphtheria outbreak that experience virulence evolution with a toxoid vaccine capable of eradicating the spread [18].

The article by [29] proposes a mathematical model to study carbon sequestration in fast growing forest plantations using fractional calculus. It uses the Mittag-Leffler function, a fractional-order operator, to characterize long-term memory effects in biomass growth, forest fires, and carbon adsorption dynamics. The model is based on rigorous mathematical method ologies such as fixed-point theory, stability analysis, and numerical simulations. The paper makes a substantial contribution to the field of environmental modeling by presenting an improved fractional-order approach to forest carbon sequestration. The mathematical approach is sound, but empirical validation and increased accessibility would improve its impact. The findings indicate that appropriate management measures, such as controlled harvesting cycles and fire suppression, can enhance carbon retention in forest plantations.

Farman et al. [8] provide a unique mathematical model to investigate fear spreading during the COVID-19 epidemic, utilizing fractional order differential equations. It employs the Caputo fractional operator and power law kernels to capture the long-term memory effects associated with emotional contagion in emergencies. The paper investigates the suggested model's well-posedness, stability, and sensitivity, resulting in a theoretical framework for understanding fear dynamics in pandemic scenarios. The article makes an important contribution to the mathematical modeling of panic spreading, especially in the setting of pandemics. It uses fractional calculus to create a more accurate model of emotional contagion dynamics. However, empirical validation and a more comprehensible presentation would increase its practical usefulness.

In [26], a fractional-order mathematical model was developed to assess the propagation and control of Ebola virus outbreaks. To reflect the disease's memory effects and complex transmission dynamics, the model employs a piecewise hybrid fractional operator in a time scale measure, in addition to the Mittag-Leffler kernel. To ensure that the model is resilient and feasible, the Lipschitz conditions, linear growth analysis, Ulam-Hyers stability, and Leray-Schauder are utilized. The work uses numerical models to assess how actions and infection rates affect disease propagation, giving useful insights for epidemic management tactics. This paper contributes significantly to mathematical epidemiology by developing a sophisticated fractional-order model of Ebola virus transmission. The integration of piecewise hybrid fractional operators and Mittag-Leffler kernels allows for a more accurate representation of the disease's memory-dependent dynamics. Theoretical rigor ensures mathematical feasibility, while numerical simulations demonstrate practical applications. However, empirical validation, computational efficiency considerations, and improved accessibility would enhance its impact.

Naik et al. [24] propose a fractional-order differential equation model to evaluate the trans mission and control of the hepatitis C virus (HCV) with memory effects. The model looks at the effects of partial immunity, treatment options, and the long-term dynamics of HCV transmission. The authors use the next-generation matrix method, the Lyapunov functional approach, and the Routh-Hurwitz stability criterion to determine the disease's overall stability. The fractional Adams-Bashforth-Moulton approach is used for numerical simulations, which support theoretical findings. This paper contributes significantly to mathematical epidemiology by developing an advanced fractional-order model for HCV transmission. The integration of memory effects and long-term immunity factors improves the accuracy of disease progression. Theoretical stability analysis and numerical simulations support the validity of the model. However, empirical validation, computational efficiency considerations, and improved accessibility would enhance its practical impact.

In [25], a fractional-order epidemic model is used to analyze the impact of co-infection with HIV and Hepatitis C Virus (HCV). The model is based on the Caputo fractional-order derivative, which efficiently accounts for memory effects and genetic characteristics

in disease transmission. The next-generation matrix approach, Lyapunov functional analysis, and Routh Hurwitz stability criteria are employed to analyze the model's global stability. Additionally, the fractional Adams Method (FAM) is employed for numerical simulations to validate the theoretical findings. This work introduces a new and robust fractional-order epidemic model for examining HIV and HCV co-infections. The memory-dependent framework offers a more realistic disease progression model, providing valuable insights into long-term infection control strategies. The research is mathematically robust, with stability proofs and numerical simulations validating the model's accuracy. However, the lack of empirical validation and practical implementation considerations limits its real-world applicability.

Naik et al. [23] developed a fractional-order mathematical model to analyze the dynamics of Hepatitis B Virus (HBV) infection, taking into account the immune response and cytokine effect. To account for memory effects during HBV development, the model uses the Caputo fractional derivative. Using Lyapunov functional methods and the Routh-Hurwitz criterion, the the model's stability, positivity, boundedness, and equilibria are studied in depth. Furthermore, the study assesses the efficacy of treatments involving nucleoside analogues and interferons, defining crucial medication efficiencies required for illness management. This paper presents a complex fractional-order model that improves our understanding of HBV infection dynamics by include immune responses and cytokine impacts. The rigorous mathematical analysis and validation through numerical simulations underscore the model's potential as a tool for exploring HBV progression and treatment strategies. However, integrating empirical data and addressing computational considerations are essential steps toward translating this theoretical framework into practical applications.

One of the methods for predicting the spread of disease using mathematical models is the Kalman filter. The Kalman Filter algorithm can be used for noise measurements in discrete time dynamic systems [4]. Having two stages, namely a prediction stage and a correction stage, the Kalman Filter is highly accurate [35]. Kalman Filters have the characteristic of being repetitive, which allows them to be used in real time [34]. The Kalman Filter method has been used to predict improvement in patients with glaucoma [11]. The spread of COVID-19 with the Kalman Filter shows that data on the spread of COVID-19 has a strong positive correlation with forecasts [30]. Effective reproduction numbers can be predicted in disease spread models using the Kalman Filter method [3]. The COVID-19 prediction in the *SEI(R)D – SD* mathematical model using the Kalman Filter for 230 days, shows that the first outbreak occurred around day 75 and the second on day 160 [19]. The spread of HIV is predicted using the Extended Kalman Filter method with antiretroviral therapy [13].

Based on the previous research, our goal of this paper is to analyze the diphtheria transmission in West Java by introducing the rates of isolation and recovery related to isolation in the quarantined populations. Moreover, to estimate the effective reproduction number of the diphtheria transmission in West Java, the implementation of Kalman Filter on the mathematical model is important to predict the trend of infected population and also effective reproduction number of Diphtheria cases. The first step of this research is to derive the effective reproduction number through the eigenvalues of next generation matrix. Moreover, we propose the sensitivity analysis of reproduction number and of each parameter of mathematical model so we can provide the effect of each parameter for the trend of susceptible, infected, quarantined, and recovered populations. Finally, the predictions are made using the Kalman Filter method to identify potential future events where these steps can prevent and control diphtheria outbreaks early.

## Method details

This paper is actually a development of the study by Fauzi et al. [9]. The diphtheria transmission model of this paper introduces a quarantined population, where the parameters of the isolation rate ( $\epsilon$ ) and the recovery rate related to isolation ( $\varphi$ ) are considered. Based on the simulation results of the diphtheria transmission model, changes in the isolation rate ( $\epsilon$ ) have a significant impact on the profiles of susceptible ( $U$ ), infected ( $V$ ), quarantined ( $W$ ), and recovered ( $Z$ ). The compartment diagram for this article is represented in Fig. 1 and the diphtheria transmission model is given in the following dynamic system Eq. (1):

$$\begin{cases} \dot{U} = (1 - \kappa p)\Lambda - \beta((1 - q) + \alpha q)UV - \mu U, \\ \dot{V} = \beta((1 - q) + \alpha q)UV - (r + \epsilon + \mu + d)V, \\ \dot{W} = \epsilon V - (\varphi + \mu + d)W, \\ \dot{Z} = \kappa p\Lambda + rV + \varphi W - \mu Z. \end{cases} \quad (1)$$

Mathematically, the parameters of  $p$ ,  $\Lambda$ ,  $\beta$ ,  $q$ ,  $\mu$ ,  $r$ ,  $\epsilon$ ,  $d$  and  $\varphi$  provide the DPT vaccination rate, the birth rate, the transmission rate, the booster vaccination rate, the natural death rate, the recovery rate related to infected, the isolation rate, the death rate related to disease and the recovery rate related to isolation respectively. Moreover, the probability of success in preventing diphtheria is expressed by  $\kappa$  and the probability of success in reducing the transmission rate of diphtheria is expressed by  $\alpha$ , where  $0 < \alpha < 1$ .

To understand the effectiveness of whether a disease is significantly infectious ( $R_0 > 1$ ) or not ( $R_0 < 1$ ), we need to find the equation of the basic reproduction number as shown below:

$$R_0 = \frac{\beta((1 - q) + \alpha q)(1 - \kappa p)\Lambda}{\mu(r + \epsilon + \mu + d)}, \quad (2)$$

where this basic reproduction number is obtained from the eigenvalues of next generation matrix (NGM) for the two matrices of the newly infected individual transmission ( $M$ ) and individual displacements transition ( $P$ ) as shown below:

$$M = \begin{pmatrix} \frac{\beta((1 - q) + \alpha q)(1 - \kappa p)\Lambda}{\mu} & 0 \\ 0 & 0 \end{pmatrix}, \quad P = \begin{pmatrix} r + \epsilon + \mu + d & 0 \\ -\epsilon & \varphi + \mu + d \end{pmatrix}.$$

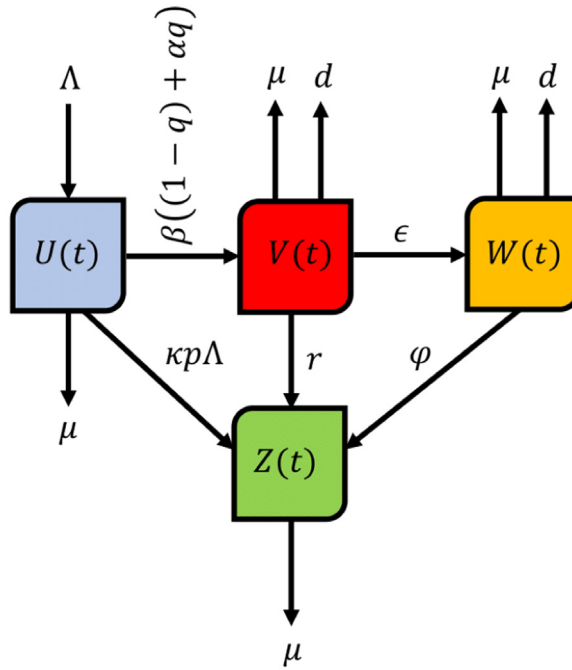


**Fig. 1.** Compartment diagram of diphtheria model.

From (2), we can conclude that the basic reproduction number is directly proportional to the transmission rate ( $\beta$ ) and inversely proportional to the natural death rate ( $\mu$ ), the recovery rate of the infected ( $r$ ), the isolation rate ( $\epsilon$ ), and the death rate due to diphtheria ( $d$ ). So, the higher the transmission rate of diphtheria, the higher the basic reproduction number, while the higher the natural death rate, the recovery rate of the infected, the isolation rate, and the death rate due to diphtheria, the lower the basic reproduction number. Moreover, the equilibrium points of disease-free ( $E^0$ ) and endemic ( $E^*$ ) are given below respectively:

$$E^0 = (U^0, V^0, W^0, Z^0) = \left( \frac{(1 - \kappa p)\Lambda}{\mu}, 0, 0, \frac{\kappa p \Lambda}{\mu} \right),$$

$$E^* = (U^*, V^*, W^*, Z^*),$$

where

$$U^* = \frac{r + \epsilon + \mu + d}{\beta((1 - q) + \alpha q)}, \quad V^* = \frac{\mu(R_0 - 1)}{\beta((1 - q) + \alpha q)}, \quad W^* = \frac{\epsilon \mu(R_0 - 1)}{\beta((1 - q) + \alpha q)(\varphi + \mu + d)},$$

$$Z^* = \frac{\kappa p \Lambda}{\mu} + \frac{(\varphi + \mu + d + \epsilon)(R_0 - 1)}{\beta((1 - q) + \alpha q)(\varphi + \mu + d)}.$$

From the equilibrium points above, the existence of free-disease is very clear, but the existence of endemic requires the value  $0 < \kappa, p < 1$  so that the basic reproduction number has positive value. Another important thing to study on the diphtheria transmission model is the significance of the parameters of the DPT vaccination rate, the birth rate, the transmission rate, the booster vaccination rate, the natural death rate, the recovery rate related to infected, the isolation rate, the death rate related to disease and the recovery rate related to isolation. The significance of these parameters is called sensitivity analysis of basic reproduction number ( $R_0$ ) as shown in the following equation:

$$S_\theta^{R_0} = \frac{\partial R_0}{\partial \theta} \times \frac{\theta}{R_0}, \quad (3)$$

where  $\theta = (p, \Lambda, \beta, q, \mu, r, \epsilon, d, \varphi)$ . Moreover, we also have the sensitivity analysis of each state variable in (1) as in the following equation:

$$S_\theta^P = \frac{\partial P}{\partial \theta} \times \frac{\theta}{P}, \quad (4)$$

where  $P = (U, V, W, Z)$ .

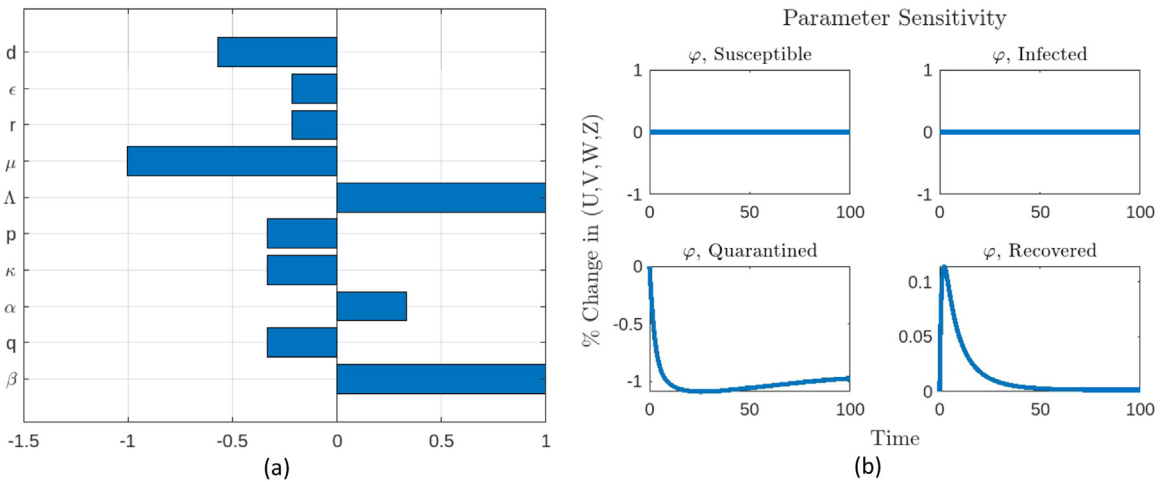


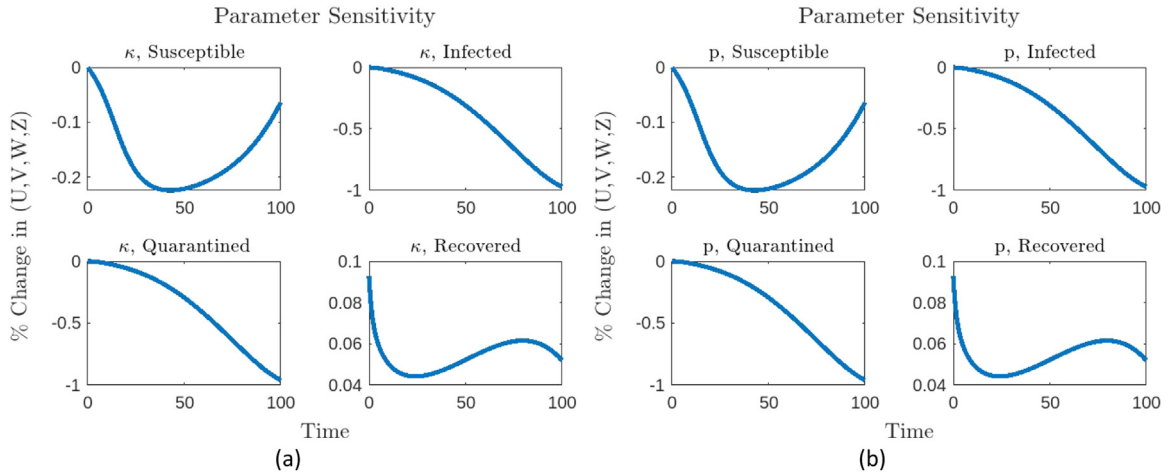
**Fig. 2.** (a): PRCC of  $R_0$ , (b): The sensitivity for parameter of  $\varphi$ .

### Method validation

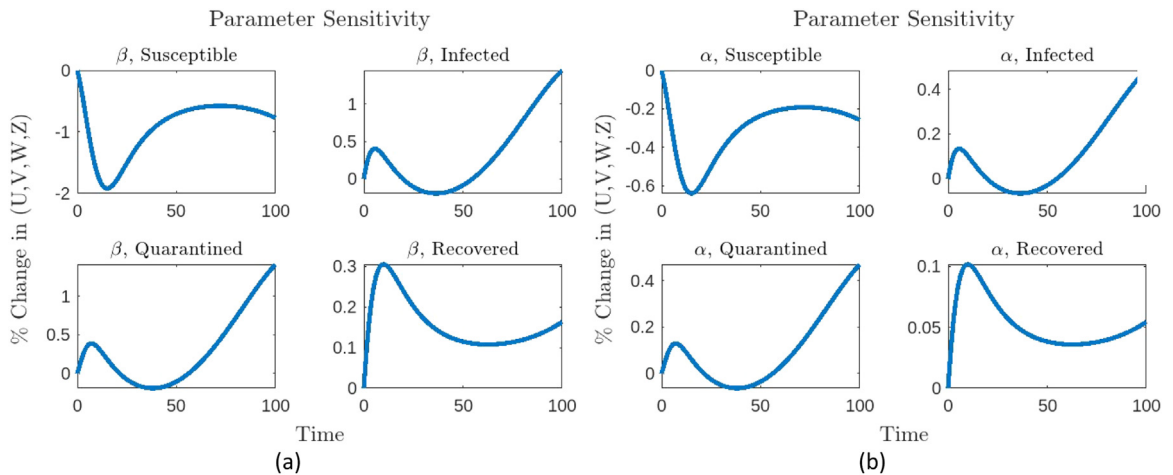
From (3) and Fig. 2a, the sensitivity indices of basic reproduction number for each parameter are given as follows:  $S_p^{R_0} = -0.333$ ,  $S_\Lambda^{R_0} = 1$ ,  $S_\beta^{R_0} = 1$ ,  $S_q^{R_0} = -0.333$ ,  $S_\mu^{R_0} = -1$ ,  $S_r^{R_0} = -0.214$ ,  $S_e^{R_0} = -0.214$ ,  $S_d^{R_0} = 0$ ,  $S_\kappa^{R_0} = -0.333$  and  $S_\alpha^{R_0} = 0.333$ . Based on the results of the sensitivity indices, three parameters ( $S_\Lambda^{R_0}$ ,  $S_\beta^{R_0}$ ,  $S_\alpha^{R_0}$ ) have a positive effect on the basic reproduction number, while seven parameters ( $S_p^{R_0}$ ,  $S_q^{R_0}$ ,  $S_\mu^{R_0}$ ,  $S_r^{R_0}$ ,  $S_e^{R_0}$ ,  $S_d^{R_0}$ ,  $S_\kappa^{R_0}$ ) have a negative effect on the basic reproduction number. Parameters ( $\Lambda$ ) and ( $\beta$ ) have a significant impact of 100 %, parameter ( $\alpha$ ) has a significant impact of 33.3 % to increase the basic reproduction number. While parameter ( $\mu$ ) has a significant impact of 100 %, parameter ( $d$ ) has a significant impact of 57 %, parameters ( $p$ ), ( $q$ ), and ( $\kappa$ ) have a significant impact of 33.3 %, parameters ( $r$ ) and ( $\epsilon$ ) have a significant impact of 21.4 %, to decrease the basic reproduction number.

Fig. 9 shows the effects of ( $R_0 < 1$ ) and ( $R_0 > 1$ ) on the profiles of susceptible, infected, quarantined, and recovered populations. ( $R_0 < 1$ ) shows that diphtheria transmission is insignificant, causing the susceptible population profile for ( $R_0 < 1$ ) to be larger than the susceptible population profile for ( $R_0 > 1$ ). The condition of ( $R_0 < 1$ ) has an impact on the susceptible population profile decreasing from the beginning to the end. The infected and quarantined population profiles when ( $R_0 < 1$ ) decrease until the number of infected and quarantined populations reaches zero. Because the profile of the infected and quarantined population when ( $R_0 < 1$ ) is smaller when compared to when ( $R_0 > 1$ ), this causes the profile of the recovered population when ( $R_0 < 1$ ) to also be smaller when compared to when ( $R_0 > 1$ ).

In contrast to Eq. (3), Eq. (4) shows the impact of each parameter on the susceptible, infected, quarantined, and recovered population profiles. Fig. 2b shows that  $\varphi$  (recovery rate related isolation) has no effect on the susceptible and infected population (this is in line with Eq. (1)). However,  $\varphi$  has an effect on reducing the number of quarantined populations initially up to 50, and after 50 the number of quarantined populations increases. Meanwhile, the effect of  $\varphi$  on the recovered population initially increases and then decreases until the end. Parameters  $\kappa$  (probability of success in preventing diphtheria) and  $p$  (DPT vaccination) have the same impact on the profile of susceptible, infected, quarantined, and recovered populations as in Fig. 3a–b. The susceptible population experiences a large decrease in the middle and increases thereafter until the end. Meanwhile, the infected and quarantined populations decrease from the beginning to the end, and the recovered population between 0–50 decreases, and above 50 increases at first then decreases until the end. Furthermore, the parameters  $\alpha$  (probability of success in reducing transmission rate of diphtheria) and  $\beta$  (infection rate) also have the same impact on the profile of susceptible, infected, quarantined, and recovered populations as in Fig. 4a–b. The infected and quarantined populations initially increase, then decrease, and finally increase again until the end. In contrast, the susceptible population decreases at the end and the recovered population is the same as the infected and quarantined populations although the increase is not as large as the infected and quarantined populations until the end. However, the parameters  $q$  (booster vaccination) and  $\Lambda$  (birth rate) have different impacts on the susceptible, infected, quarantined, and recovered population profiles as shown in Fig. 5a–b. Booster vaccination causes the infected, quarantined, and recovered population profiles to decrease at the end even though they initially increase. This is different from the birth rate which causes the infected, quarantined, and recovered population profiles to increase from the beginning to the end. The profile of susceptible population has the opposite effect from the other profiles for  $q$  and  $\Lambda$ , namely  $q$  causes the susceptible population to increase at the end and  $\Lambda$  causes the susceptible population to decrease at the end. Parameters  $r$  (recovery rate related to infected),  $\epsilon$  (isolation rate), and  $d$  (death rate related to disease) have the same impact but parameter  $\mu$  (natural death rate) on the susceptible, infected, quarantined, and recovered population profiles as in Fig. 6a–b and Fig. 7a–b. Parameter  $\mu$  causes the infected, quarantined, and recovered population profiles to be decreased from the beginning to the



**Fig. 3.** (a)-(b): The sensitivity for parameters of  $\kappa$  and  $p$  respectively.



**Fig. 4.** (a)-(b): The sensitivity for parameters of  $\beta$  and  $\alpha$  respectively.

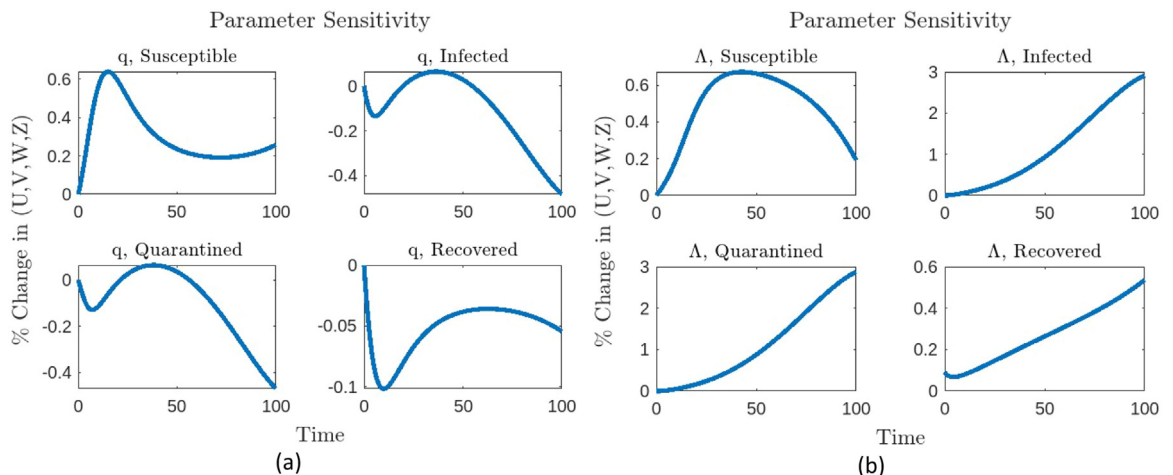


**Fig. 5.** (a)-(b): The sensitivity for parameters of  $q$  and  $\Lambda$  respectively.

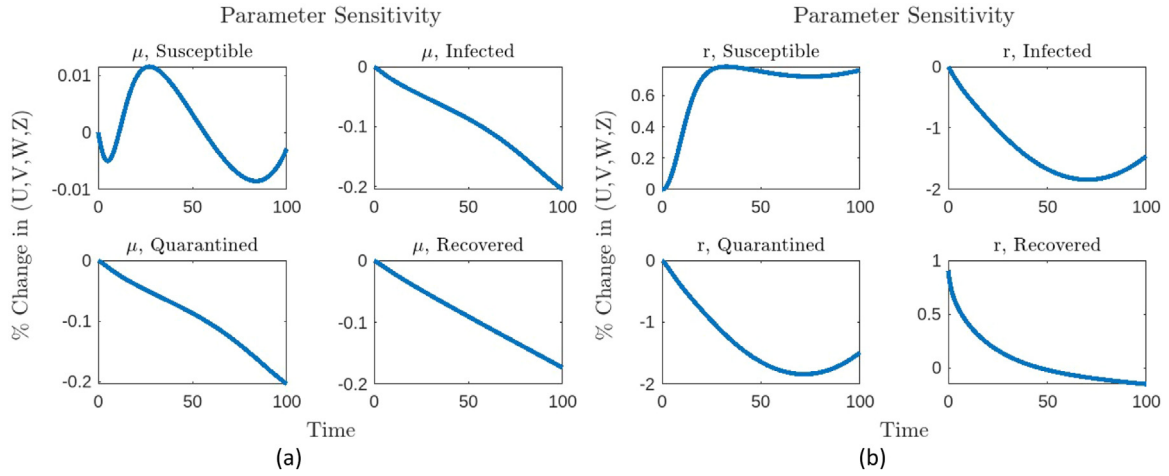


**Fig. 6.** (a)-(b): The sensitivity for parameters of  $\mu$  and  $r$  respectively.

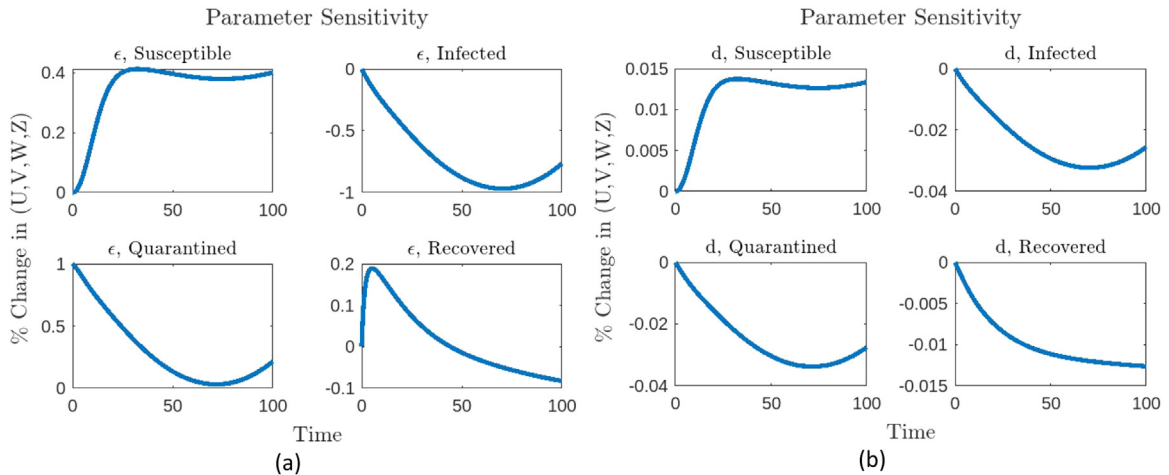


**Fig. 7.** (a)-(b): The sensitivity for parameters of  $\epsilon$  and  $d$  respectively.

end. However, parameters  $r$ ,  $\epsilon$ , and  $d$  cause the recovered profile to decrease from the beginning to the end. In contrast, the infected and quarantined profiles increase at the end even though they initially decrease for parameters  $r$ ,  $\epsilon$ , and  $d$ . The highest peak of the susceptible population is between 0–50 and the lowest peak is between 50–100 for the parameter  $\mu$ , while for the parameters  $r$ ,  $\epsilon$ , and  $d$ , the highest peak is between 0–50 and at the end.

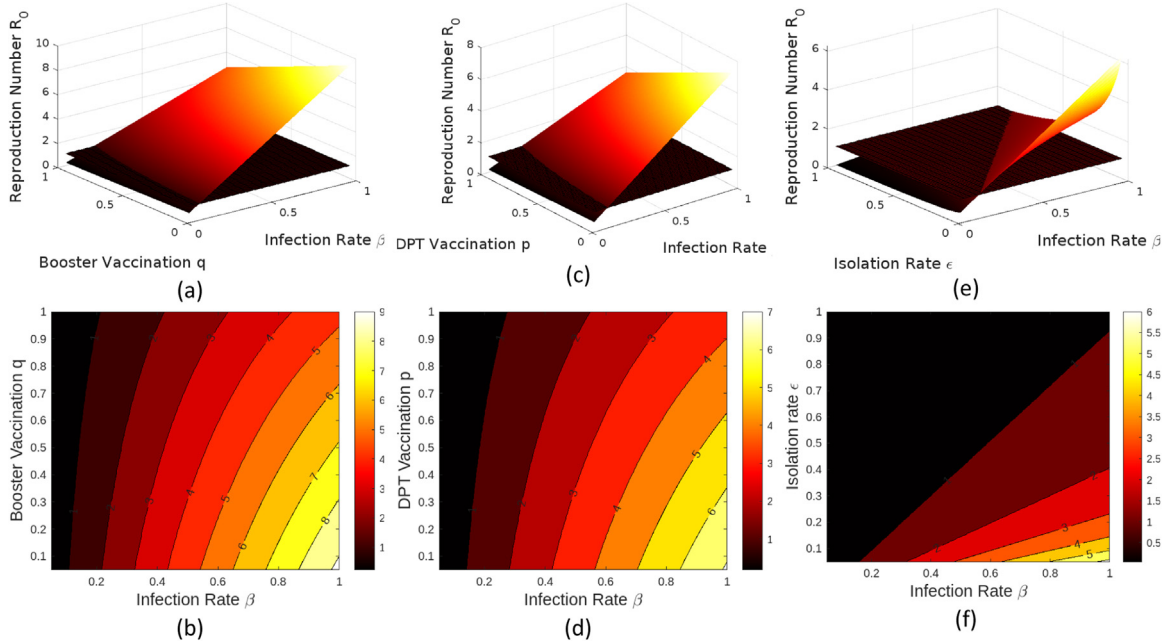
Eq. (2) shows the reproduction number for fixed values of all parameters. Next, we want to see the trend of the basic reproduction number changing over time. For this reason, we modify the second equation of (1) to be as follows where the infection rate changes over time:

$$\beta(t) = \frac{\frac{dV(t)}{dt} + (r + \epsilon + \mu + d)V(t)}{((1 - q) + \alpha q)U(t)V(t)}. \quad (5)$$

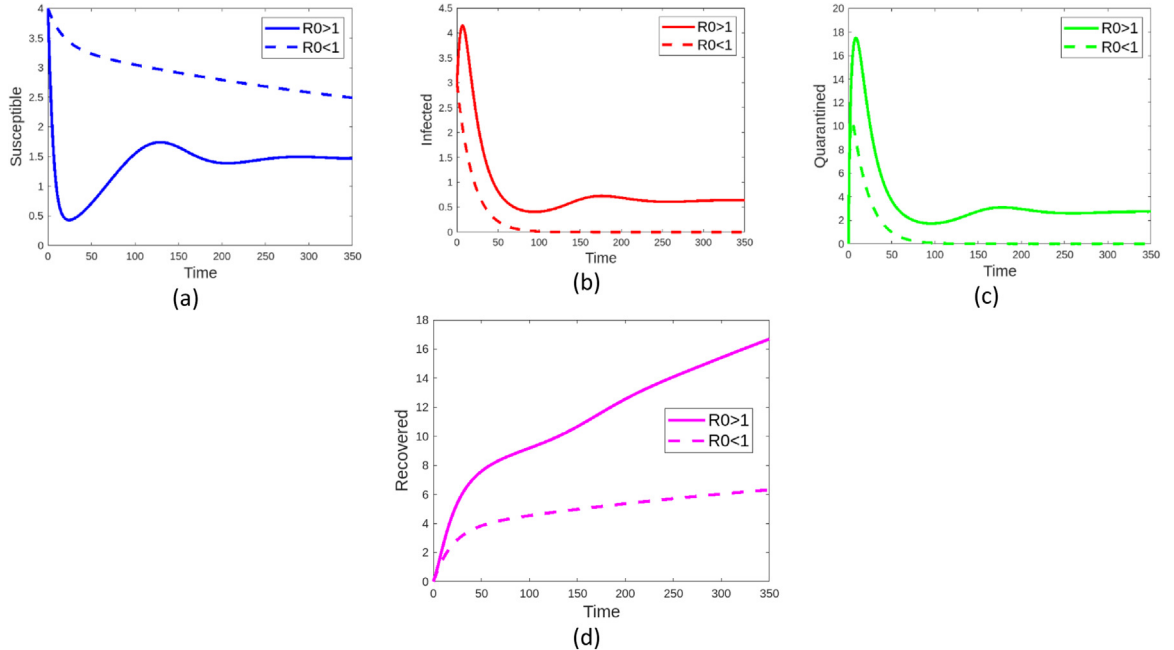
Due to the positiveness of all parameters and state variables, then the infection rate is also positive for all times  $t > 0$ , i.e.,  $\beta(t) > 0$ . From Eq. (5), for all times  $t > 0$ , the basic reproduction number in (2) can be stated as in the following equation:

$$R_0(t) = \frac{\beta(t)((1 - q) + \alpha q)(1 - \kappa p)\Lambda}{\mu(r + \epsilon + \mu + d)}, \quad (6)$$

Fig. 8 shows the correlation between the infection rate and booster vaccination, the infection rate and DPT vaccination, and the infection rate and isolation rate, on the basic reproduction number. Based on the three correlations, the isolation rate gives the smallest reproduction number, followed by DPT vaccination, and finally booster vaccination. In this case, the implementation of isolation is an effective step for the infected population to suppress diphtheria transmission. Meanwhile, booster vaccination has a

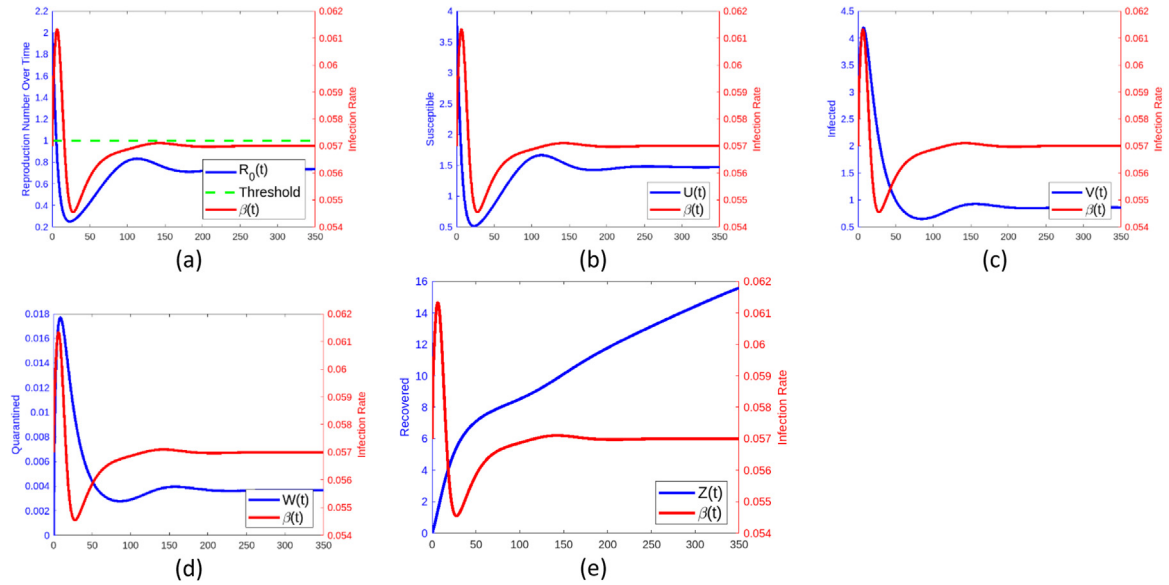


**Fig. 8.** (a)-(b):  $R_0(q, \beta)$ , (c)-(d):  $R_0(p, \beta)$ , (e)-(f):  $R_0(\epsilon, \beta)$ .



**Fig. 9.** The profiles of  $U, V, W, Z$  for endemic ( $R_0 > 1$ ) and disease-free ( $R_0 < 1$ ).

smaller impact when compared to DPT vaccination in reducing diphtheria transmission, this is because DPT vaccination is a basic vaccination so that with the presence of vaccination it will form antibodies for the body of diphtheria sufferers. As a result, booster vaccination does not have much effect in reducing diphtheria transmission when compared to DPT vaccination. Furthermore, these results can also be seen from the contour. The dark area shows a small reproduction number. This means that the wider the dark area, the smaller the reproduction number (the more effective the parameter is in reducing diphtheria transmission) Fig. 8(f) (isolation rate) shows the largest dark area, followed by Fig. 8(d) (DPT vaccination), and finally Fig. 8(b) (booster vaccination).



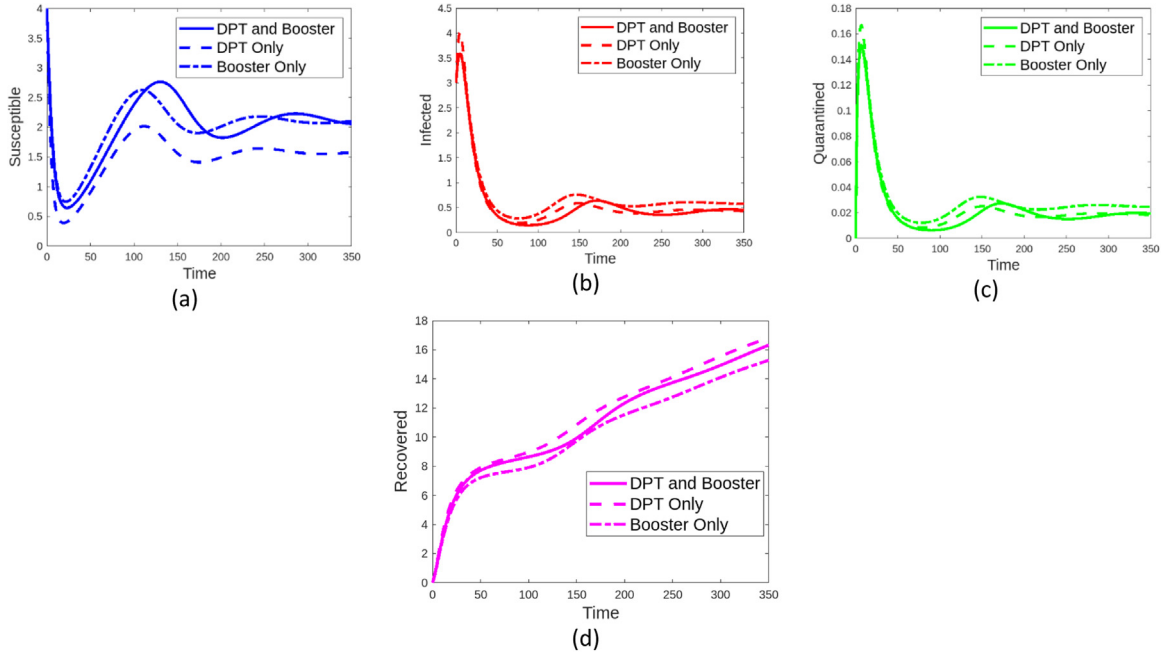
**Fig. 10.** (a)-(e): The profiles of correlations between infection rate ( $\beta(t)$ ) and basic reproduction number ( $R_0(t)$ ), between infection rate ( $\beta(t)$ ) and susceptible populations ( $U(t)$ ), between infection rate ( $\beta(t)$ ) and infected populations ( $V(t)$ ), between infection rate ( $\beta(t)$ ) and quarantined populations ( $W(t)$ ) and between infection rate ( $\beta(t)$ ) and recovered populations ( $Z(t)$ ) respectively.

Fig. 10a shows the trend of changes in the basic reproduction number due to the infection rate which also changes over time. We can see that the basic reproduction number and the infection rate have the same trend over time and also the highest peak value is similar. When the infection rate decreases, the basic reproduction number also decreases and when the infection rate is constant, this is also similar to the constant basic reproduction number. From a time of 150–350, both the infection rate and the basic reproduction number, experience a fairly constant trend (and their values are below 1 which is the threshold of the basic reproduction number). The trend of the infection rate also has the same effect on the profiles of susceptible, infected, quarantined, and recovered as in Fig. 10b–e. Because the infection rate has a positive effect on the infected population, as seen in Fig. 10c, when the infection rate decreases, the decrease for the infected population is much more gradual when compared to the trend of the infection rate, but at the end it also experiences a constant trend. However, it is different with the recovery profile, where when the infection rate is constant, the profile experiences a constant increase. This is likely because the infection rate does not directly affect the dynamics of the recovered population. A constant infection rate has an impact on the number of populations that are increasing significantly.

Figs. 11–12 show the effect of the combination of (DPT and booster), (DPT only), and (booster only) on the susceptible, infected, quarantined, and recovered population profiles with variations in isolation rate ( $\epsilon = 0.03$  and  $\epsilon = 0.003$ ). From Eq. (1), the isolation rate has a positive effect on the quarantined population profile and a negative effect on the infected population profile. This causes the scale of the infected population profile when ( $\epsilon = 0.03$ ) to be smaller than when ( $\epsilon = 0.003$ ). This is different from the quarantined population profile, where the parameter ( $\epsilon = 0.03$ ) gives a larger quarantined population profile when compared to when ( $\epsilon = 0.003$ ). From Figs. 11–12 gives the same trend from the combination of (DPT and booster), (DPT only), and (booster only). DPT only causes the susceptible, infected, and quarantined population profiles to be smaller when compared to the use of booster only. This indicates that the use of booster only has a less significant effect in reducing the susceptible, infected, and quarantined population profiles and this is likely when using DPT only the body forms antibodies against diphtheria. While the recovery population profile is higher when using DPT only compared to booster only. The combination of DPT and boosters almost gives the same effect as DPT only, so in this case it starts from the ineffectiveness of using boosters to reduce diphtheria transmission.

In fact, Fig. 13 confirms the results in Figs. 11–12 for the combination of (DPT and booster), (DPT only), and (booster only) with variations in isolation rate ( $\epsilon = 0.03$  and  $\epsilon = 0.003$ ). Because isolation rate has a positive effect on the profile of the quarantined population, the difference in isolation rate values ( $\epsilon = 0.03$  and  $\epsilon = 0.003$ ) has a very significant impact as in Fig. 13c. The use of DPT only gave the smallest mean value for the susceptible population profile (followed by the combination of DPT and booster and booster only), gave the second smallest mean value (starting with the combination of DPT and booster, and third with booster only) for the profile of infected population, and quarantined gave the largest mean value for the recovered population profile (followed by the combination of DPT and booster, and last with booster only).

Inadequate immunization coverage, restricted access to health care, and a lack of public knowledge all contribute to the spread of preventable diseases such as diphtheria. During COVID-19, health resources and attention were redirected to combat the epidemic, which could have an impact on diphtheria surveillance, diagnosis, and treatment. Because of its dense human population, West Java Province is regarded as one of Indonesia's highest risk places for diphtheria infection. With a big number of people living close together,



**Fig. 11.** The profiles of  $U, V, W, Z$  for DPT and Booster, DPT only and Booster only (isolation rate  $\epsilon = 0.03$ ).

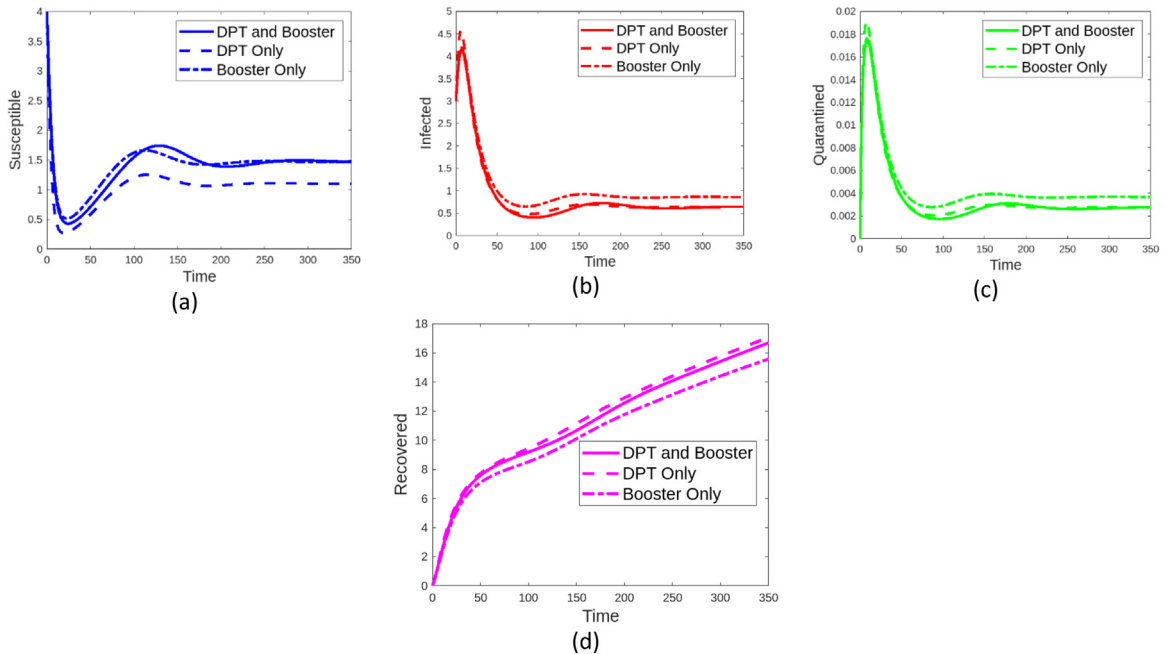


**Fig. 12.** The profiles of  $U, V, W, Z$  for DPT and Booster, DPT only and Booster only (isolation rate  $\epsilon = 0.003$ ).

the possibility of diphtheria bacteria transmission increases. Crammed and congested living environments can help the disease spread, particularly in places with poor access to health care and low vaccination rates. The West Java Provincial Health Office's health profile shows that the number of diphtheria infections grew considerably in 2016. Unfortunately, diphtheria cases in many locations of West Java have increased since the COVID-19 pandemic. Fig. 14a shows that the pattern of monthly case accumulation in West Java rose from January 2021 to April 2023. The booster vaccination contains diphtheria antigen, which reminds the immune system of its initial training and keeps it prepared to respond promptly to any potential diphtheria exposure. The combination of DPT 1, DPT 2, DPT

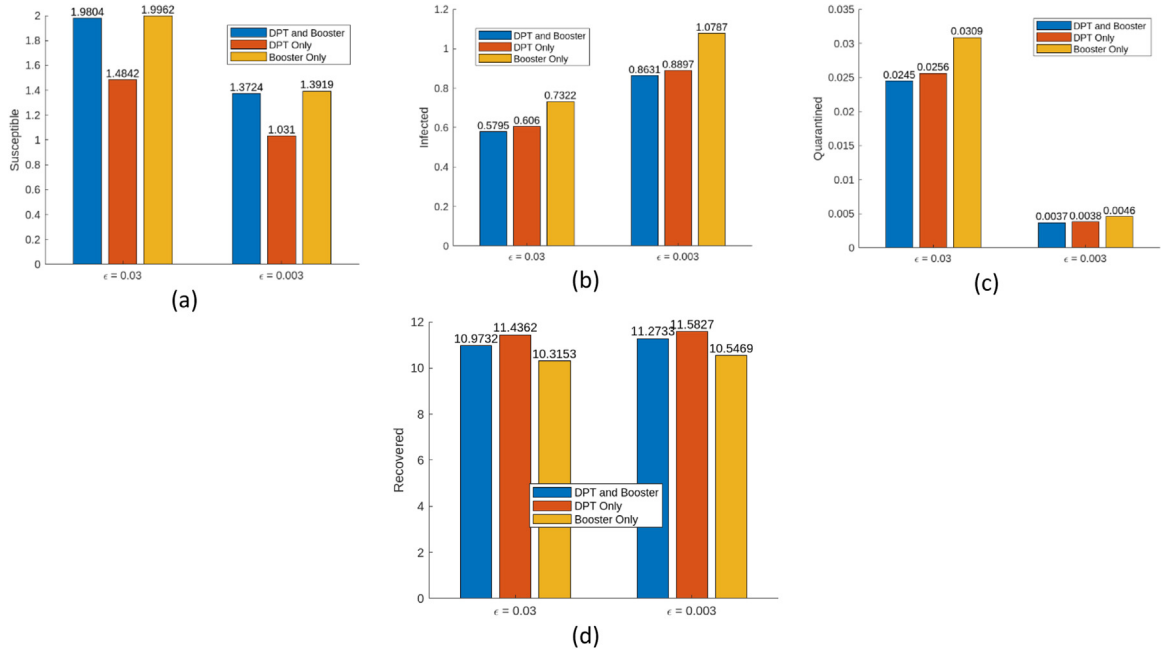


**Fig. 13.** The mean values of  $U, V, W, Z$  for DPT and Booster (Blue), DPT only (Red) and Booster only (Yellow) with the isolation rates  $\epsilon = 0.03$  and  $\epsilon = 0.003$ .

3, and booster vaccine gives long-term immunity and robust resistance against diphtheria, protecting people and improving overall public health by lowering the risk of diphtheria transmission. In recent years, the province of West Java has enhanced public health services for diphtheria through a comprehensive vaccination program. The DPT vaccine has reduced the incidence of diphtheria in all regions of West Java. Geographic inequalities, cultural attitudes, and limited access to health services make it difficult for West Java to sustain high immunization coverage in all regions. However, DPT and booster vaccine coverage has remained reasonably high over the last eight years. Fig. 14b shows the coverage of DPT and booster vaccinations in West Java.

Next, we study the trend of the basic reproduction number for diphtheria transmission cases in West Java, with fixed parameters  $\varphi = 0.7$ ,  $\Lambda = 0.07$ ,  $\alpha = 0.5$ ,  $\beta = 0.057$ ,  $\mu = 0.0019$ ,  $r = 0.057$ ,  $\epsilon = 0.003$ ,  $d = 0.001$ ,  $\kappa = 0.5$ ,  $p = 0.05$ , and  $q = 0.05$ . Generally, the flowchart of Extended Kalman Filter is represented in Fig. 15 where this method consists of update and predict steps.  $F(\hat{Y}(\zeta|\zeta))$  is the right-hand side of our system and  $J(\hat{Y}(\zeta|\zeta))$  is the Jacobian matrix of our system. The new estimate of state variable is iteratively updated using Kalman gain  $K(\zeta + 1)$  until the maximum iteration is reached. The estimation results of the basic reproduction number are divided into three cases: booster only, DPT only, and a combination of DPT and booster. As in Fig. 16b-d, the estimation results produced are good and this is also based on the values of RMSE, NRMSE, and MAPE which are quite small in Table 2. Meanwhile, Fig. 16e shows the trends of the basic reproduction number and the infection rate, where the trend of the infection rate is directly proportional to the trend of the basic reproduction number. Around the scale of 0-7 (2021 January to 2021 July) the basic reproduction number is still below 1 (the threshold of the basic reproduction number). This means that in that range the transmission of diphtheria is not too significant. However, when the scale is 8-27 (2021 August to 2023 March) the trend of the reproduction number continues to rise until it exceeds the threshold limit, which means that in that range the transmission of diphtheria is very significant, which is in line with the actual data on diphtheria cases which continue to increase in West Java. From Fig. 16b-d, DPT only gives the smallest basic reproduction number when compared to the basic reproduction number produced by booster only and the combination of DPT and booster. This result is also in line with our model analysis (without actual data) where DPT only has a very significant impact in reducing the level of significance of diphtheria transmission, which is due to the possibility of the body forming an immune system when DPT only is given. Fig. 16a and Table 1 are the reasons why the use of the Extended Kalman Filter is quite significant in estimating the basic reproduction number based on actual data on diphtheria cases in West Java. The metric performance of Kalman filter based on the diphtheria transmission model can be stated as follows:

$$RMSE = \sqrt{\frac{1}{N} \sum_{j=1}^N (\hat{Y}_j - Y_j)^2}, \quad NRMSE = \sqrt{\frac{\frac{1}{N} \sum_{j=1}^N (\hat{Y}_j - Y_j)^2}{\bar{Y}_j}},$$

$$MAPE = \frac{1}{N} \sum_{j=1}^N \frac{|\hat{Y}_j - Y_j|}{Y_j} \times 100\%,$$

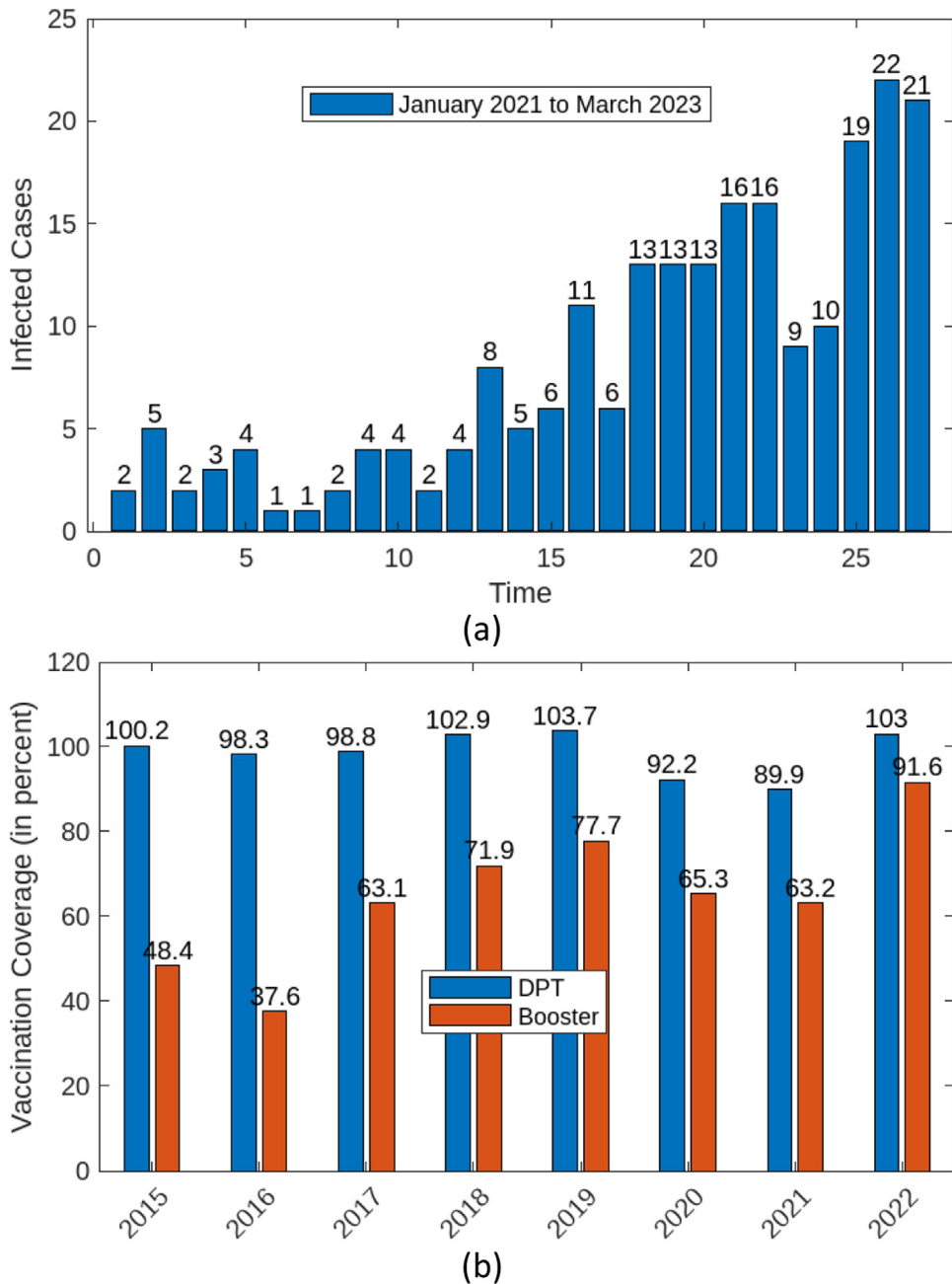


**Fig. 14.** (a): The monthly actual data (the detailed time is listed in Table 1) and (b): The annual vaccination coverage where all data sources are from the study in [9].

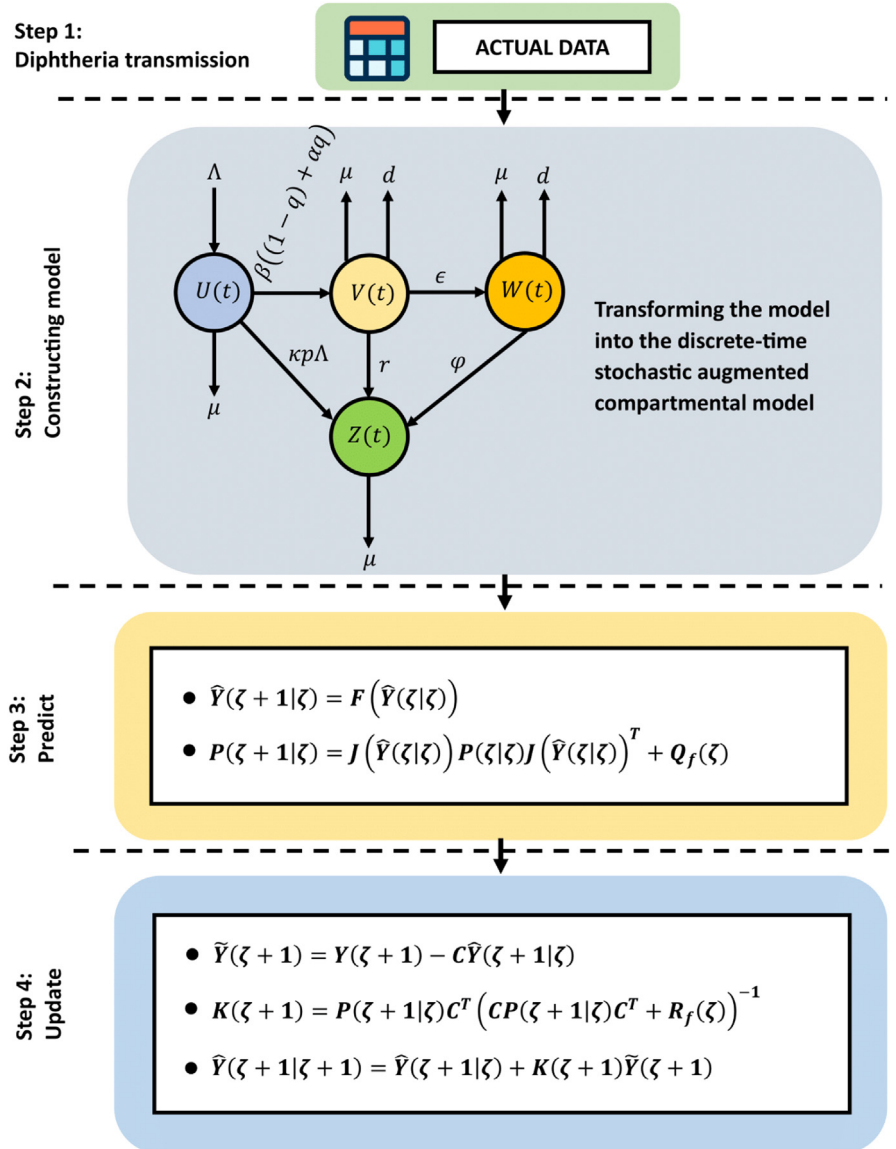


**Fig. 15.** Extended Kalman filter based on the diphtheria transmission model.

where  $\hat{Y}_j$  and  $Y_j$  show the predicted results and actual data respectively, while  $\bar{Y}_j$  is the mean value of actual data. The Jacobian matrix of dynamical system (1) is given below:

$$J(\hat{Y}) = \begin{pmatrix} M_{11} & M_{12} & M_{13} & M_{14} \\ M_{21} & M_{22} & M_{23} & M_{24} \\ M_{31} & M_{32} & M_{33} & M_{34} \\ M_{41} & M_{42} & M_{43} & M_{44} \end{pmatrix},$$

where

$$M_{11} = 1 - \Delta t((\beta(1-q) + \alpha\beta q)\hat{V} - \mu), \quad M_{12} = -\beta\Delta t((1-q) + \alpha q)\hat{U}, \quad M_{13} = 0, \quad M_{14} = 0,$$

$$M_{21} = \beta\Delta t((1-q) + \alpha q)\hat{V}, \quad M_{22} = 1 + \Delta t((\beta(1-q) + \alpha\beta q)\hat{U} - (r + \epsilon + \mu + d)), \quad M_{23} = 0, \quad M_{24} = 0,$$

$$M_{31} = 0, \quad M_{32} = 0, \quad M_{33} = 1 - \Delta t(\varphi + \mu + d), \quad M_{34} = 0,$$

$$M_{41} = 0, \quad M_{42} = r\Delta t, \quad M_{43} = \varphi\Delta t, \quad M_{44} = -\mu\Delta t.$$

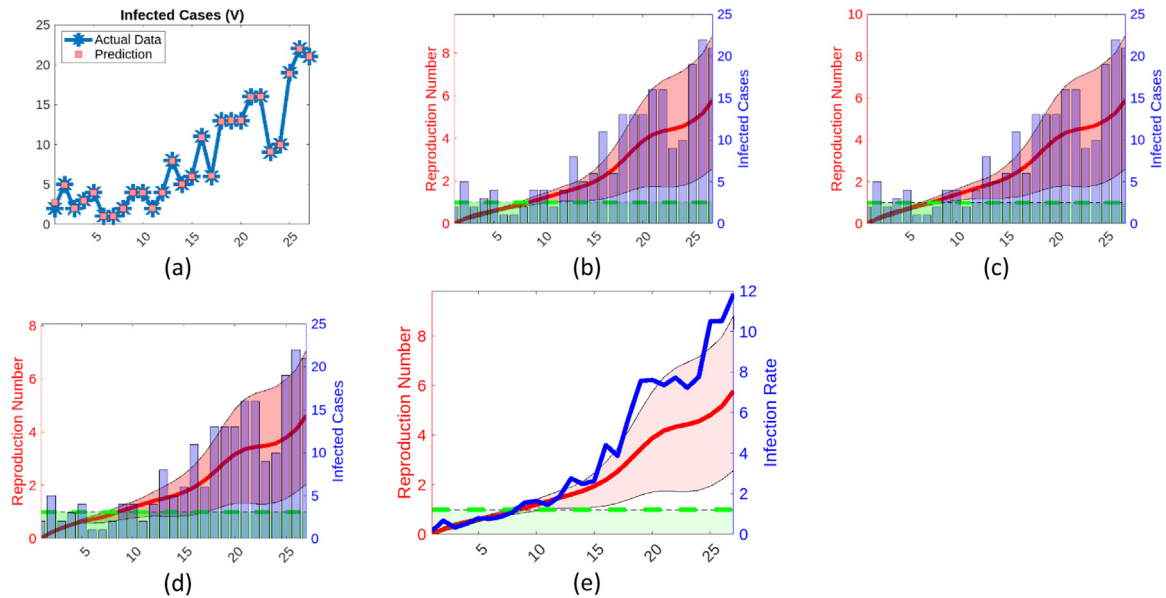


**Fig. 16.** (a): The predicted profiles using extended Kalman filter, (b): Reproduction number (DPT and Booster vaccinations), (c): Reproduction number (Booster vaccination only), (d): Reproduction number (DPT vaccination only), and (e): Correlations of  $(R_0(t), \beta(t))$ .

**Table 1**

The actual data (**B**) and predictions for DPT only (**C1**), Booster only (**D1**) and DPT and Booster (**E1**) and the differences for DPT only (**C2**), Booster only (**D2**) and DPT and Booster (**E2**) respectively based on the observation period (**A**).

No	A	B	C		D		E	
			C1	C2	D1	D2	E1	E2
1	2021 January	2	2.7593	0.7593	2.7592	0.7592	2.7592	0.7592
2	2021 February	5	4.9489	-0.0511	4.9483	-0.0517	4.9482	-0.0518
3	2021 March	2	2.0471	0.0471	2.0470	0.0470	2.0470	0.0470
4	2021 Apr	3	2.9820	-0.0180	2.9818	-0.0182	2.9817	-0.0183
5	2021 May	4	3.9819	-0.0181	3.9815	-0.0185	3.9813	-0.0187
6	2021 June	1	1.0480	0.0480	1.0479	0.0479	1.0479	0.0479
7	2021 July	1	0.9995	-0.0005	0.9995	-0.0005	0.9994	-0.0006
8	2021 August	2	1.9831	-0.0169	1.9829	-0.0171	1.9828	-0.0172
9	2021 September	4	3.9670	-0.0330	3.9663	-0.0337	3.9661	-0.0339
10	2021 October	4	3.9994	-0.0006	3.9988	-0.0012	3.9985	-0.0015
11	2021 November	2	2.0319	0.0319	2.0317	0.0317	2.0315	0.0315
12	2021 December	4	3.9674	-0.0326	3.9668	-0.0332	3.9664	-0.0336
13	2021 January	8	7.9373	-0.0627	7.9357	-0.0643	7.9350	-0.0650
14	2022 February	5	5.0490	0.0490	5.0484	0.0484	5.0480	0.0480
15	2022 March	6	5.9846	-0.0154	5.9840	-0.0160	5.9834	-0.0166
16	2022 Apr	11	10.9272	-0.0728	10.9251	-0.0749	10.9241	-0.0759
17	2022 May	6	6.0839	0.0839	6.0833	0.0833	6.0827	0.0827
18	2022 June	13	12.9012	-0.0988	12.8990	-0.1010	12.8978	-0.1022
19	2022 July	13	13.0210	0.0210	13.0186	0.0186	13.0175	0.0175
20	2022 August	13	13.0201	0.0201	13.0184	0.0184	13.0174	0.0174
21	2022 September	16	15.9737	-0.0263	15.9726	-0.0274	15.9715	-0.0285
22	2022 October	16	16.0233	0.0233	16.0224	0.0224	16.0214	0.0214
23	2022 November	9	9.1248	0.1248	9.1246	0.1246	9.1240	0.1240
24	2022 December	10	9.9978	-0.0022	9.9974	-0.0026	9.9967	-0.0033
25	2023 January	19	18.8960	-0.1040	18.8926	-0.1074	18.8914	-0.1086
26	2023 February	22	21.9976	-0.0024	21.9950	-0.0050	21.9938	-0.0062
27	2023 March	21	21.0659	0.0659	21.0630	0.0630	21.0619	0.0619

## Conclusions

Based on the results and discussions, we are concerned with investigating the trend of the basic reproduction number on diphtheria transmission in West Java for three scenarios: DPT only, booster only, and a combination of DPT and booster. The extended Kalman filter approach produces considerable results in calculating the basic reproduction number based on actual data of diphtheria cases

**Table 2**

The validations between model and actual data.

DPT Only			Booster Only			DPT and Booster		
RMSE	NRMSE	MAPE	RMSE	NRMSE	MAPE	RMSE	NRMSE	MAPE
0.1551	0.0189	15.52 %	0.0189	0.0189	2.56 %	0.1552	0.0189	2.51 %

in West Java, as measured by RMSE, NRMSE, and MAPE values. Based on those the performance analysis for DPT only, booster only, and a combination of DPT and booster respectively as in [Table 2](#), we can conclude that extended Kalman filter provide a good estimation on the model of diphtheria transmission.

In this paper, we also looked at the quarantined population because the rate of isolation has a major impact on the profiles of susceptible, infected, quarantined, and recovered populations. According to the data, DPT only delivers the smallest number when compared to Booster only or the combinations of Booster and DPT. The body probably develops an immune system when DPT only is employed, which is why the booster itself does not significantly decrease the effectiveness of diphtheria transmission (for the lower basic reproduction number). From [Fig. 16.](#), it provides that isolation rate is directly proportional to the effective reproduction number and the DPT only presents the lowest the effective reproduction number than the others (the DPT only provides the highest impact than Booster only and a combination of DPT and booster).

## Limitations

The Diphtheria model of this paper only focuses on integer order, the system is only able to capture the current state. In fact, the growth rate of the population is not only able to capture the current state but also the effects of memory and long-rate interactions. In this case, the model needs to be modified in fractional order.

## Ethics statements

As an expert scientist and along with co-authors of the concerned field, the paper has been submitted with full responsibility, following due ethical procedure, and there is no duplicate publication, fraud, plagiarism, or concerns about animal or human experimentation.

## CRediT author statement

**Mohammad Ghani:** Conceptualization, Formal analysis, Investigation, Writing – original draft, Writing – review and editing, Software.

## Declaration of competing interest

The author declares that the author has no known competing financial interests or personal relationships that could have appeared to influence the work reported in this paper.

## Data availability

Data will be made available on request.

## Acknowledgments

The author would like to thank the reviewers for their valuable comments and suggestions which helped to improve the paper.

## References

- [1] O.A. Adegbeye, et al., A resurgence and re-emergence of diphtheria in Nigeria, 2023, Ther. Adv. Infect. Dis. 10 (2023) 1–4, doi:[10.1177/20499361231161936](https://doi.org/10.1177/20499361231161936).
- [2] E.B. Akponana, E.O. Arierhie, N.J. Egbinne, A.M. Okedoye, Mathematical modelling of diphtheria transmission dynamics for effective strategies of prevention and control with emphasis on vaccination and vaccine-induced immunity, Int. J. Res. Eng. Sci. 1 (4) (2023).
- [3] F. Arroyo-Marioli, F. Bullano, S. Kucinskas, C. Rond'ón-Moreno, Tracking R of COVID-19: a new real-time estimation using the Kalman filter, PLoS. One 16 (1 January) (2021) 1–16, doi:[10.1371/journal.pone.0244474](https://doi.org/10.1371/journal.pone.0244474).
- [4] M.A. Akram, P. Liu, M.O. Tahir, W. Ali, Y. Wang, A state optimization model based on kalman filtering and robust estimation theory for fusion of multi-source information in highly non-linear systems, Sensors (Switzerland) 19 (7) (2019), doi:[10.3390/s19071687](https://doi.org/10.3390/s19071687).
- [5] S. O'Boyle, et al., National public health response to an outbreak of toxigenic Corynebacterium diphtheriae among asylum seekers in England, 2022: a descriptive epidemiological study, Lancet Public Heal 8 (10) (2023) e766–e775, doi:[10.1016/S2468-2667\(23\)00175-5](https://doi.org/10.1016/S2468-2667(23)00175-5).
- [6] B. Cheuvart, M. Burgess, F. Zepp, J. Mertsola, J. Wolter, L. Schuerman, Anti diphtheria antibody seroprotection rates are similar 10 years after vaccination with dTpa or DTaP using a mathematical model, Vaccine 23 (3) (2004) 336–342, doi:[10.1016/j.vaccine.2004.06.012](https://doi.org/10.1016/j.vaccine.2004.06.012).
- [7] K.E.N. Clarke, A. MacNeil, S. Hadler, C. Scott, T.S.P. Tiwari, T. Cherian, Global epidemiology of diphtheria, Updat. Myopia A Clin. Perspect. 25 (10) (2019) 1834–1842 [N]. Available:, doi:[10.3201/eid2510.190271](https://doi.org/10.3201/eid2510.190271).

- [8] M. Farman, et al., A sustainable method for analyzing and studying the fractional-order panic spreading caused by the COVID-19 pandemic, *Partial Differ. Equ. Appl. Math.* 13 (101047) (2025) 1–19, doi:[10.1016/j.padiff.2024.101047](https://doi.org/10.1016/j.padiff.2024.101047).
- [9] I.S. Fauzi, et al., Assessing the impact of booster vaccination on diphtheria transmission: mathematical modeling and risk zone mapping, *Infect. Dis. Model.* 9 (1) (2024) 245–262, doi:[10.1016/j.idm.2024.01.004](https://doi.org/10.1016/j.idm.2024.01.004).
- [10] F. Finger, et al., “Real-time analysis of the diphtheria outbreak amongst forcibly displaced Myanmar nationals in Bangladesh,” *bioRxiv*, vol. 7, pp. 1–11, 2018, [Online]. Available: <https://f1000research.com/slides/7-631>
- [11] G.P. Garcia et al., “Patients with normal tension glaucoma,” pp. 111–119, 2020.
- [12] M. Ghani, I.Q. Utami, F.W. Triyayuda, M. Afifah, A fractional SEIQR model on diphtheria disease, *Model. Earth Syst. Environ.* 9 (2) (2023) 2199–2219, doi:[10.1007/s40808-022-01615-z](https://doi.org/10.1007/s40808-022-01615-z).
- [13] P. Di Giambardino, D. Iacoviello, Early estimation of the number of hidden HIV infected subjects: an extended Kalman filter approach, *Infect. Dis. Model.* 8 (2) (2023) 341–355, doi:[10.1016/j.idm.2023.03.001](https://doi.org/10.1016/j.idm.2023.03.001).
- [14] A. Hempenstall, J. Short, V. Fisher, C. Taunton, A. Preston-Thomas, T. Marquardt, Toxigenic diphtheria cases in North Queensland, Australia, *Popul. Med.* 5 (Supplement) (2023), doi:[10.18332/popmed/165756](https://doi.org/10.18332/popmed/165756).
- [15] Z. Islam, S. Ahmed, M.M. Rahman, M.F. Karim, M.R. Amin, Global stability analysis and parameter estimation for a diphtheria model: a case study of an epidemic in Rohingya Refugee camp in Bangladesh, *Comput. Math. Methods Med.* 2022 (2022), doi:[10.1155/2022/6545179](https://doi.org/10.1155/2022/6545179).
- [16] W. de Jong, T. Asmarawati, E.C.M. van Gorp, M. Goeijenbier, *A diphtheria case in indonesia: a future foe to Europe?* *Neth. J. Med.* 78 (1) (2020) 41–43.
- [17] S. Kanchanarat, S. Chinviriyasit, W. Chinviriyasit, Mathematical assessment of the impact of the imperfect vaccination on diphtheria transmission dynamics, *Symmetry, (Basel)* 14 (10) (2022), doi:[10.3390/sym14102000](https://doi.org/10.3390/sym14102000).
- [18] F. Lecorvaisier, D. Pontier, B. Soubeyrand, D. Fouchet, Using a dynamical model to study the impact of a toxoid vaccine on the evolution of a bacterium: the example of diphtheria, *Ecol. Modell.* 487 (2024) 110569, doi:[10.1016/j.ecolmodel.2023.110569](https://doi.org/10.1016/j.ecolmodel.2023.110569).
- [19] R. Lal, W. Huang, Z. Li, An application of the ensemble Kalman filter in epi demiological modelling, *PLoS. One* 16 (8 August) (2021) Aug., doi:[10.1371/journal.pone.0256227](https://doi.org/10.1371/journal.pone.0256227).
- [20] C.E. Madubueze, K.A. Tijani, Fatmawati, A deterministic mathematical model for optimal control of diphtheria disease with booster vaccination, *Healthc. Anal.* 4 (July) (2023) 100281, doi:[10.1016/j.health.2023.100281](https://doi.org/10.1016/j.health.2023.100281).
- [21] K.K. Maramraj, et al., Addressing reemergence of diphtheria among adolescents through program integration in india, *Emerg. Infect. Dis.* 27 (3) (2021) 953–956, doi:[10.3201/eid2703.203205](https://doi.org/10.3201/eid2703.203205).
- [22] H. Martini, et al., Diphtheria in Belgium: 2010–2017, *J. Med. Microbiol.* 68 (10) (2019) 1517–1525, doi:[10.1099/JMM.0.001039](https://doi.org/10.1099/JMM.0.001039).
- [23] P.A. Naik, et al., Global analysis of a fractional-order Hepatitis B virus model under immune response in the presence of cytokines, *Adv. Theory Simul.* 7 (2400726) (2024), doi:[10.1002/adts.202400726](https://doi.org/10.1002/adts.202400726).
- [24] P.A. Naik, et al., Memory impacts in hepatitis C: a global analysis of a fractional-order model with an effective treatment, *Comput. Methods Programs Biomed.* 254 (108306) (2024) 1–17, doi:[10.1016/j.cmpb.2024.108306](https://doi.org/10.1016/j.cmpb.2024.108306).
- [25] P.A. Naik, et al., Modeling and analysis of the fractional-order epidemic model to investigate mutual influence in HIV/HCV co-infection, *Nonlinear. Dyn.* 112 (11679) (2024) 11679–11710, doi:[10.1007/s11071-024-09653-1](https://doi.org/10.1007/s11071-024-09653-1).
- [26] P.A. Naik, et al., Modeling and analysis using piecewise hybrid fractional operator in time scale measure for ebola virus epidemics under Mittag-Leffler kernel, *Sci. Rep.* 14 (24963) (2024) 1–23, doi:[10.1038/s41598-024-75644-2](https://doi.org/10.1038/s41598-024-75644-2).
- [27] J.O. Omojuigbe, P.O. Aluko, D.T. Omojuigbe, T. Oluwajomiloko, B.O. Odedeyi, and V.O. Oloyede, “Re-emergence of diphtheria outbreak in Nigeria: efforts, challenges and recommendations,” vol. 6, no. 1, 2024.
- [28] M. Salman, et al., Re-emergence of diphtheria after COVID-19 pandemic in Pakistan: time to consider booster vaccination strategies, *J. Infect.* 88 (5) (2024) 106141, doi:[10.1016/j.jinf.2024.106141](https://doi.org/10.1016/j.jinf.2024.106141).
- [29] M.U. Saleem, et al., Modeling and analysis of a carbon capturing system in forest plantations engineering with Mittag-Leffler positive invariant and global Mittag-Leffler proper ties, *Modeling Earth Syst. Environ.* 11 (38) (2024) 11–38, doi:[10.1007/s40808\\_024-02181-2](https://doi.org/10.1007/s40808_024-02181-2).
- [30] K.K. Singh, S. Kumar, P. Dixit, M.K. Bajpai, Kalman filter based short term prediction model for COVID-19 spread, *Appl. Intell.* 51 (5) (2021) 2714–2726, doi:[10.1007/s10489-020-01948-1](https://doi.org/10.1007/s10489-020-01948-1).
- [31] K. Sornbundit, W. Triampo, C. Modchang, Mathematical modeling of diphtheria transmission in Thailand, *Comput. Biol. Med.* 87 (2017) 162–168, doi:[10.1016/j.combiomed.2017.05.031](https://doi.org/10.1016/j.combiomed.2017.05.031).
- [32] S.A. Truelove, et al., Clinical and epidemiological aspects of diphtheria: a systematic review and pooled analysis, *Clin. Infect. Dis.* 71 (1) (2020) 89–97, doi:[10.1093/cid/ciz808](https://doi.org/10.1093/cid/ciz808).
- [33] R. Tosepu, J. Gunawan, D.S. Effendy, L.O.A.I. Ahmad, A. Farzan, The outbreak of diphtheria in Indonesia, *Pan Afr. Med. J.* 31 (2018) 1–5, doi:[10.11604/pamj.2018.31.249.16629](https://doi.org/10.11604/pamj.2018.31.249.16629).
- [34] C. Urrea, R. Agramonte, Kalman filter: historical overview and review of its use in robotics 60 years after its creation, *J. Sens.* 2021 (2021) Hindawi Limited, doi:[10.1155/2021/9674015](https://doi.org/10.1155/2021/9674015).
- [35] B. Wang, Z. Sun, X. Jiang, J. Zeng, R. Liu, Kalman filter and its application in data assimilation, *Atmosphere (Basel)* 14 (8) (2023), doi:[10.3390/atmos14081319](https://doi.org/10.3390/atmos14081319).
- [36] D. Weerasekera, J. M'oller, M.E. Kranner, C.A. Antunes, A.L. Mattos-Guaraldi, A. Burkowski, Beyond diphtheria toxin: cytotoxic proteins of corynebacterium ulcerans and corynebacterium diphtheriae, *Microbiol. (United Kingdom)* 165 (8) (2019) 876–890, doi:[10.1099/mic.0.000820](https://doi.org/10.1099/mic.0.000820).